Inorganic Chemistry

Communication

Cite This: Inorg. Chem. XXXX, XXX, XXX-XXX

pubs.acs.org/IC

Concave $ZnFe_2O_4$ Hollow Octahedral Nanocages Derived from Fe-Doped MOF-5 for High-Performance Acetone Sensing at Low-Energy Consumption

Xue-Zhi Song,[†] Yu-Lan Meng,[†] Zhenquan Tan,[†] Liang Qiao,[†] Teng Huang,[†] and Xiao-Feng Wang*[,‡]

[†]School of Petroleum and Chemical Engineering and [‡]School of Mathematics and Physics Science, Dalian University of Technology, 2 Dagong Road, Liaodongwan New District, Panjin 124221, Liaoning China

Supporting Information

ABSTRACT: Herein, through a morphology-inherited annealing treatment of a hollow Fe-doped MOF-5 octahedron as the self-sacrificing template, we report the synthesis of concave $ZnFe_2O_4$ hollow octahedral nanocages as sensing materials, which exhibited high performance, including unprecedented excellent sensitivity, good selectivity, and cyclic stability at ultralow working temperature (120 °C).

Acetone, a hazardous chemical gas, can cause skin and eye irritation, mood swings, and nausea and anesthetize the central nervous system.[1,2] Therefore, it is of great significance and urgency to fabricate a highly efficient acetone gas sensor for environmental monitoring and human health protection.

Chemiresistive gas sensors based on transition-metal oxide (TMO) semiconductors have been paid more and more attention because of their low cost, synthetic ease, facile integration and portability, and excellent sensing ability, rendering them as superior techniques over other gas detection methods.[3,4] Up to now, single TMOs, TMO composites, and single-phase multi-TMOs as sensing materials integrated into prospective sensors have been successfully fabricated.[5−12] $ZnFe_2O_4$, a typical n-type semiconductor nanomaterial, has been used in many fields as a photodegradation catalyst, an anode material in lithium-ion batteries, and electrocatalyst for hydrogen evolution reaction and even overall water splitting.[13−18] Notably, great endeavors dedicated to optimizing the microstructures of $ZnFe_2O_4$, including yolk−shell microspheres, nanosheet-assembled hollow microspheres, porous nanospheres, mesoporous materials, and nanotubes, have been made to improve the gas-sensing performances.[19−23] Notwithstanding the achievements, the sometimes complicated or high-energy consumption synthetic process of sensing materials, the unsatisfactory gas-sensing sensitivity, and the high operating temperature of the sensors restrict their scalable and really practical application. The enlarged surface area, the promotion of permeability, and the improvement of the utility factor of the sensing body will achieve superior TMO-based gas analyzers because gas sensing involves a surface reaction between the target gas and sensing materials. Thus, the porous hollow structures are envisaged to be excellent candidates as advanced sensing materials.

Hollow nanostructures have earned much more attention for their intriguing structure-induced properties and applications in catalysis, drug delivery, energy storage/conversion, and many other fields.[24−27] Previously, Wang et al. demonstrated that the sensing behavior of hollow microspheres, especially for multi-shell hollow structures with higher specific area, outperformed that of the bulk counterparts.[28] Besides other well-developed synthetic technologies,[29,30] however, the most powerful and conventional strategy to generate porous and hollow TMOs relies on the thermal decomposition of hollow metal−organic framework (MOF) precursors. Recently, MOFs have been chosen as versatile precursors or sacrificial templates for the synthesis of TMO nanomaterials, which have been used in the electrocatalysis and energy storage fields.[31−35] Nevertheless, the research of porous TMOs from MOFs as gas sensors is still in its infancy.[36−38] By choosing $Zn_3[Fe(CN)_6]_2{\cdot}xH_2O$ as the precursor, our group has just synthesized $ZnO/ZnFe_2O_4$ triple-shelled hollow microspheres as high-performance sensors toward acetone.[39] Despite numerous fruits about MOF nanomaterials, only a few of the hollow MOFs were presented, for instance, zeolitic imidazolate framework (ZIF-8) nanobubbles, multi-shelled hollow chromium(III) terephthalate MOFs (MIL-101), and well-defined Fe^{III}-MOF-5 hollow nanocages, by a selective etching process and a surface-energy-driven mechanism.[40−42]

As a proof of concept, we herein propose the hollow bimetallic MOF precursor-directed synthesis of concave $ZnFe_2O_4$ porous hollow octahedral nanocages by thermal decomposition (Scheme 1). As sensing materials, the integrated chemiresistive gas sensor can deliver a high sensitivity of 64.4 toward 200 ppm

Scheme 1. Schematic Preparation Process of Concave Porous Hollow $ZnFe_2O_4$ Octahedral Nanocages

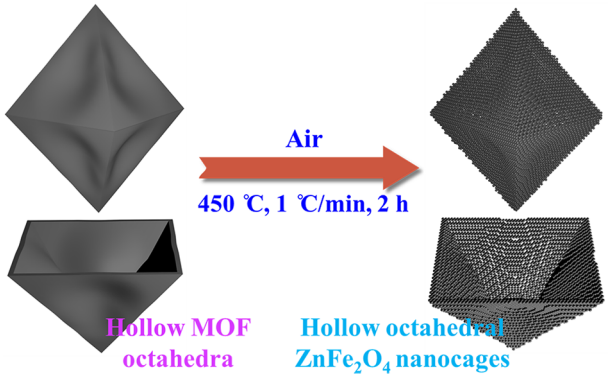

Received: September 22, 2017

ACS Publications © XXXX American Chemical Society

DOI: 10.1021/acs.inorgchem.7b02425
Inorg. Chem. XXXX, XXX, XXX−XXX

acetone vapor. Remarkably, it also shows excellent selectivity and good cyclic stability.

Well-defined Fe^{III}-doped MOF-5 hollow octahedra as the starting self-sacrificial templates were synthesized through a one-pot solvothermal method.[42] No obvious diffraction peak in the powder X-ray diffraction (PXRD) pattern reveals that these octahedra are typically amorphous (Figure S2), which refers to infinite coordination polymers.[43] A panoramic field-emission scanning electron microscopy (FESEM) image displayed in Figure 1a clearly demonstrates that well-defined uniform MOF

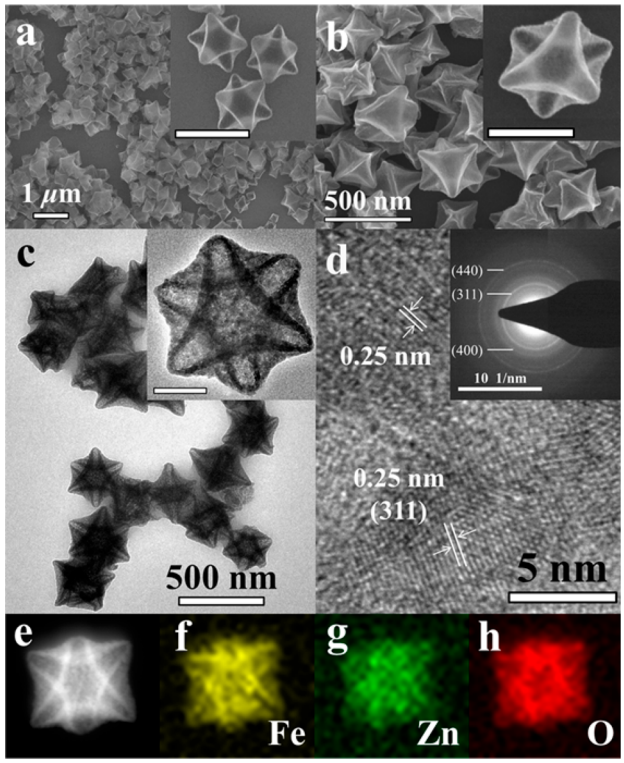

Figure 1. (a) SEM images of an Fe^{III}-doped MOF-5 precursor (inset scale bar 500 nm). (b) SEM images (inset scale bar 250 nm), (c) TEM images (inset scale bar 100 nm), (d) HRTEM images, with the inset showing the SAED pattern, (e) HAADF-STEM image, (f–h) Energy-dispersive spectroscopy elemental mapping images of $ZnFe_2O_4$ octahedral nanocages.

particles with an average size of around 280 nm (an average edge length of 240 nm) were obtained. From the magnified FESEM image, the different contrast in the octahedral particle with a smooth surface reveals that it is hollow (Figure 1a, inset). A transmission electron microscopy (TEM) image further discloses the hollow nature of these octahedral nanostructures, consistent with the high-angle annular dark-field scanning transmission electron microscopy (HAADF-STEM) image (Figure S3). The homogeneous coexistence of the Fe and Zn elements in the precursor provides the synthetic possibility of a multimetal oxide after an annealing treatment in air. The broadening PXRD peaks of the annealed product can be indexed to cubic spinel $ZnFe_2O_4$ (JCPDS 65-3111), also suggesting a nanocrystalline nature with ultrafine crystallite sizes. Interestingly, the annealed product well preserves the original octahedral morphology of the precursor. It is notable that the surfaces of the octahedral nanocages are quite rough and more acutely inward compared to the precursor because of the stress difference caused by gas release and the diffusion discrepancy in the rate and distance of O_2 flux from the surface/edges (Figure 1b).[44] TEM observations revealed that the shell (a thickness of approximately 26 nm) of the concave hollow nanocage consisted of a large number of ultrafine nanoparticles of ≈6–9 nm size (Figure 1c). The nanoparticle building blocks are homogeneously distributed with interconnected, numerous pores left. This appealing porous hollow feature would greatly favor for generation of more reactive sites and acceleration of mass transport. Clear lattice fringes with a spacing of ≈0.25 nm in the high-resolution TEM (HRTEM) image can be indexed to the (311) lattice plane of the spinel $ZnFe_2O_4$ (Figure 1d). Moreover, the selected-area electron diffraction (SAED) pattern (Figure 1d, inset) with a series of concentric rings reveals the polycrystalline characteristics and corresponds well to the (440), (400), and (311) planes of $ZnFe_2O_4$. The elemental mapping images (Figure 1f–h) evidently reveal the homogeneous distribution of the Zn, Fe, and O elements throughout the whole hollow nanocage. The X-ray photoelectron microscopy (XPS) survey spectrum (Figure S5) also suggests the presence of the Zn, Fe and O elements in the final $ZnFe_2O_4$ nanocages. The fitting peaks in the high-resolution Zn 2p spectrum centered at ≈1044.37 and ≈1021.3 eV corresponding to Zn $2p_{1/2}$ and Zn $2p_{3/2}$, respectively, reveal the Zn^{II} oxidation state to be in line with the octahedral site (B site) of $ZnFe_2O_4$. The binding energies (BEs) for Fe $2p_{3/2}$ at ≈712.9 and ≈711.0 eV are assigned to the tetrahedral (A site) and octahedral (B site) sites, respectively. Moreover, another two peaks at ≈725.0 and ≈719.2 eV are attributed to Fe $2p_{1/2}$ and the shakeup satellite structure, respectively. All of the above results verify the Fe^{III} oxidation state in the $ZnFe_2O_4$ phase. The high-resolution XPS spectrum of O 1s can be deconvoluted into two peaks at BEs of ≈531.47 and ≈529.86 eV, which are characteristic of surface-adsorbed oxygen species, such as $O_2^-{}_{ads}$ and $O^-{}_{ads}$, and a surface lattice oxygen (O^{2-}), respectively.[45] The adsorbed oxygen species are the reactive species with target gas molecules, playing a significant role in the improvement of the gas-sensing performances.[46] The high Brunauer–Emmett–Teller (BET) specific surface area of the final $ZnFe_2O_4$ nanocages was calculated to be 150.5 $m^2 \cdot g^{-1}$. The pore size distributed hierarchically and concentrated around 2.7, 4.0, 6.8, and 13.1 nm, indicating a mesoporous characteristic (Figures S6). Such a mesoporous hollow nanocage with high specific surface area would provide ample reactive sites and facilitate target gas diffusion, enabling the construction of a high-performance sensor device.

The temperature-dependent sensing behavior of a gas sensor based on as-prepared $ZnFe_2O_4$ hollow octahedral nanocages was first investigated to disclose its optimum operating temperature because the temperature affects gas adsorption/desorption processes and surface reactions. As shown in Figure 2a, with an increase in the operating temperature, the responses toward all of the tested gases display an "increase–maximum–decrease" tendency. At a low temperature, the reaction between the tested gas molecules and surface-adsorbed oxygen species was too inert to give a high response. As the operating temperature increased, the test gas molecules were activated enough to overcome the activation energy barrier to react with more surface-absorbed oxygen species, leading to a significantly enhanced response. Because of the low utilization rate of the sensing material caused by limited gas adsorption and diffusion, the response of the sensor was reduced at higher temperature. The optimum operating temperature of 120 °C was applied for further investigations of the sensing performance because the largest response to an acetone value higher than those of other

DOI: 10.1021/acs.inorgchem.7b02425
Inorg. Chem. XXXX, XXX, XXX–XXX

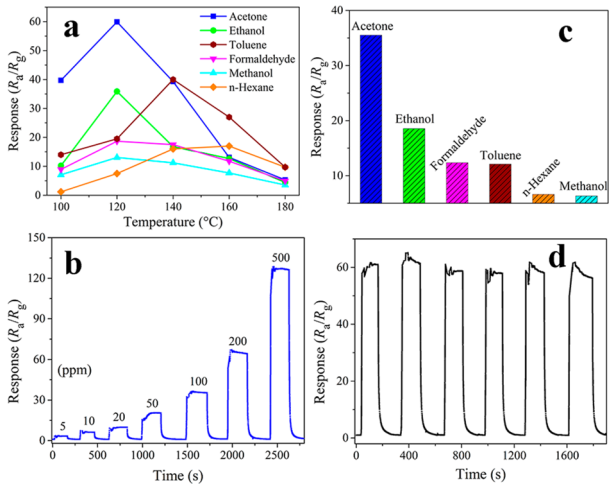

Figure 2. (a) Response of the sensor to different gases (200 ppm) at different working temperatures. (b) Dynamic response−recovery transients of the sensor to acetone at different concentrations. (c) Responses of the gas sensor to various gases (100 ppm). (d) Reproducibility of the sensor on successive exposure to 200 ppm acetone.

counterparts was achieved. With increasing acetone concentration, the response values increased significantly from 3.27, 6.27, 9.71, 20.51, 35.52, and 64.42 to 127.06 at concentrations of 5, 10, 20, 50, 100, 200, and 500 ppm, respectively, observed from the dynamic response−recovery transients in Figure 2b.

Compared with other previously relevant acetone gas sensors (Table S1), such as $ZnFe_2O_4$ nanoparticles (39.5, 200 ppm, and 200 °C),[47] $ZnFe_2O_4$ yolk−shell microspheres (near 40.5, 100 ppm, and 200 °C),[19] $ZnFe_2O_4$−ZnO composite hollow microspheres (20.8, 200 ppm, and 320 °C)[48] and $ZnFe_2O_4$ nanosheets on ZnO hollow spheres (16.8, 100 ppm, and 250 °C),[49] our sensor response value is much higher or comparable to the above examples at much lower working temperature, rendering it as a highly sensitive, safer, really applied gas sensor at low-energy consumption. The appealing highly sensitive sensing ability may be ascribed to the high BET surface area, porous feature, and nanoparticle building block size comparable with the electron depletion layer thickness of hollow $ZnFe_2O_4$ nanocages, favoring more active oxygen species, gas diffusion, and complete depletion, which are in agreement with the three key factors (the receptor function, utility factor, and transducer function) in semiconductor oxide gas sensors proposed by Yamazoe et al.[50,51]

A bar graph in Figure 2c shows a comparison of the responses of the sensor toward various gases (acetone, ethanol, formaldehyde, toluene, methanol, and hexane) at 100 ppm concentration to demonstrate the good selectivity because the response toward acetone is remarkably higher as opposed to those of the other counterparts (at least about twice that of ethanol). The response−recovery behavior could be well-repeated with no clear attenuation in response upon alternate exposure to air and 200 ppm acetone gas for several cycles, which indicates the superb robustness and repeatability of the as-fabricated sensor (Figure 2d).

The most accepted sensing mechanism of n-type semiconductor oxide $ZnFe_2O_4$ belongs to the surface-controlled model, which is based on a resistance change of the semiconductive sensor caused by the adsorption/desorption of different gaseous molecules. In an air atmosphere, oxygen molecules would be adsorbed on the surface of $ZnFe_2O_4$ hollow nanocages to form active oxygen species ($O_2^-{}_{ads}$, $O^-{}_{ads}$, and $O^{2-}{}_{ads}$) by capturing electrons from the conduction bands of $ZnFe_2O_4$, resulting in a thick electron depletion layer, a relatively high potential barrier on the surface region, and a high resistance. After the introduction of a reducing gas, the acetone molecules could react with the former active oxygen species to generate CO_2 and H_2O and reinject the trapped electrons back to the conduction band, consequently reducing the electron depletion layer thickness and lowering the resistance of the sensor (Figure 3).

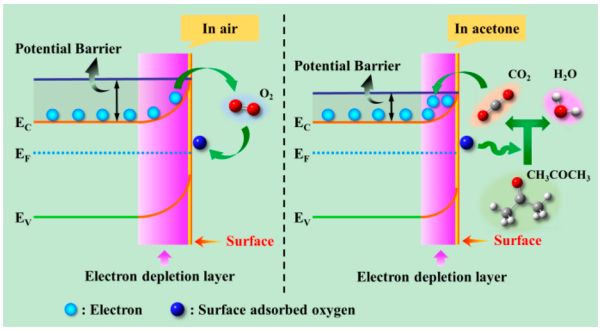

Figure 3. Schematic diagram of the acetone sensing mechanism.

In summary, through annealing treatment of hollow Fe-doped MOF-5 octahedra, concave $ZnFe_2O_4$ hollow octahedral nanocages have been successfully prepared with high specific surface area and porous nanostructures assembled by nanoparticles as primary building blocks. As a sensing material, this chemiresistive sensor possesses unprecedentedly high sensitivity with its response value of 64.4−200 ppm acetone, as well as good selectivity and cyclic stability at an ultralow working temperature (120 °C). This work may pave the way toward a universal fabricative methodology of an advanced gas sensor based on TMO nanomaterials from proper MOF nanoprecursors.

■ ASSOCIATED CONTENT

Supporting Information

The Supporting Information is available free of charge on the ACS Publications website at DOI: 10.1021/acs.inorgchem.7b02425.

Experimental section, TEM images, XPS spectra, and PXRD patterns (PDF)

■ AUTHOR INFORMATION

Corresponding Author

*E-mail: wangxf@dlut.edu.cn.

ORCID

Zhenquan Tan: 0000-0002-1730-7290

Xiao-Feng Wang: 0000-0002-5413-4798

Notes

The authors declare no competing financial interest.

■ ACKNOWLEDGMENTS

The authors are grateful for financial support from the National Natural Science Foundation of China (Grants 21601027, 51602035, and 21571028), the Fundamental Research Funds for the Central Universities [Grants DUT17LK33 and DUT16RC(4)69], and the Xinghai Scholars Program from Dalian University of Technology.

DOI: 10.1021/acs.inorgchem.7b02425
Inorg. Chem. XXXX, XXX, XXX−XXX

REFERENCES

(1) Cao, W.; Duan, Y. Breath analysis: potential for clinical diagnosis and exposure assessment. *Clin. Chem.* **2006**, *52*, 800−811.

(2) Grelet, C.; Bastin, C.; Gelé, M.; Davière, J.-B.; Johan, M.; Werner, A.; Reding, R.; Fernandez Pierna, J. A.; Colinet, F. G.; Dardenne, P.; Gengler, N.; Soyeurt, H.; Dehareng, F. Development of Fourier transform mid-infrared calibrations to predict acetone, β-hydroxybutyrate, and citrate contents in bovine milk through a European dairy network. *J. Dairy Sci.* **2016**, *99*, 4816−4825.

(3) Wagner, T.; Haffer, S.; Weinberger, C.; Klaus, D.; Tiemann, M. Mesoporous materials as gas sensors. *Chem. Soc. Rev.* **2013**, *42*, 4036−4053.

(4) Zhao, Z.; Tian, J.; Sang, Y.; Cabot, A.; Liu, H. Structure, synthesis, and applications of TiO_2 nanobelts. *Adv. Mater.* **2015**, *27*, 2557−2582.

(5) Xu, J.; Pan, Q.; Shun, Y.; Tian, Z. Grain size control and gas sensing properties of ZnO gas sensor. *Sens. Actuators, B* **2000**, *66*, 277−279.

(6) Zhou, X.; Feng, W.; Wang, C.; Hu, X.; Li, X.; Sun, P.; Shimanoe, K.; Yamazoe, N.; Lu, G. Porous ZnO/$ZnCo_2O_4$ hollow spheres: synthesis, characterization, and applications in gas sensing. *J. Mater. Chem. A* **2014**, *2*, 17683−17690.

(7) Chen, Y. J.; Zhu, C. L.; Wang, L. J.; Gao, P.; Cao, M. S.; Shi, X. L. Synthesis and enhanced ethanol sensing characteristics of α-Fe_2O_3/SnO_2 core-shell nanorods. *Nanotechnology* **2009**, *20*, 045502.

(8) Huang, H.; Gong, H.; Chow, C. L.; Guo, J.; White, T. J.; Tse, M. S.; Tan, O. K. Low-temperature growth of SnO_2 nanorod arrays and tunable n-p-n sensing response of a ZnO/SnO_2 heterojunction for exclusive hydrogen sensors. *Adv. Funct. Mater.* **2011**, *21*, 2680−2686.

(9) Li, C. C.; Yin, X. M.; Li, Q. H.; Wang, T. H. Enhanced gas sensing properties of ZnO/SnO_2 hierarchical architectures by glucose-induced attachment. *CrystEngComm* **2011**, *13*, 1557−1563.

(10) Sun, P.; Cai, Y.; Du, S.; Xu, X.; You, L.; Ma, J.; Liu, F.; Liang, X.; Sun, Y.; Lu, G. Hierarchical α-Fe_2O_3/SnO_2 semiconductor composites: Hydrothermal synthesis and gas sensing properties. *Sens. Actuators, B* **2013**, *182*, 336−343.

(11) Bao, M.; Chen, Y.; Li, F.; Ma, J.; Lv, T.; Tang, Y.; Chen, L.; Xu, Z.; Wang, T. Plate-like p-n heterogeneous NiO/WO_3 nanocomposites for high performance room temperature NO_2 sensors. *Nanoscale* **2014**, *6*, 4063−4066.

(12) Jeong, H. M.; Kim, J. H.; Jeong, S. Y.; Kwak, C. H.; Lee, J. H. Co_3O_4-SnO_2 hollow heteronanostructures: facile control of gas selectivity by compositional tuning of sensing materials via galvanic replacement. *ACS Appl. Mater. Interfaces* **2016**, *8*, 7877−7883.

(13) Guo, Y.; Zhang, N.; Wang, X.; Qian, Q.; Zhang, S.; Li, Z.; Zou, Z. A facile spray pyrolysis method to prepare Ti-doped $ZnFe_2O_4$ for boosting photoelectrochemical water splitting. *J. Mater. Chem. A* **2017**, *5*, 7571−7577.

(14) Liu, B.; Li, X.; Zhao, Q.; Hou, Y.; Chen, G. Self-templated formation of $ZnFe_2O_4$ double-shelled hollow microspheres for photocatalytic degradation of gaseous *o*-dichlorobenzene. *J. Mater. Chem. A* **2017**, *5*, 8909−8915.

(15) Zhang, Y.; Shi, Q.; Schliesser, J.; Woodfield, B. F.; Nan, Z. Magnetic and thermodynamic properties of nanosized Zn ferrite with normal spinal structure synthesized using a facile method. *Inorg. Chem.* **2014**, *53*, 10463−10470.

(16) Sun, M.; Chen, Y.; Tian, G.; Wu, A.; Yan, H.; Fu, H. Stable mesoporous $ZnFe_2O_4$ as an efficient electrocatalyst for hydrogen evolution reaction. *Electrochim. Acta* **2016**, *190*, 186−192.

(17) Hwang, H.; Shin, H.; Lee, W. J. Effects of calcination temperature for rate capability of triple-shelled $ZnFe_2O_4$ hollow microspheres for lithium ion battery anodes. *Sci. Rep.* **2017**, *7*, 46378.

(18) Mady, A. H.; Baynosa, M. L.; Tuma, D.; Shim, J.-J. Facile microwave-assisted green synthesis of Ag-$ZnFe_2O_4$@rGO nanocomposites for efficient removal of organic dyes under UV- and visible-light irradiation. *Appl. Catal., B* **2017**, *203*, 416−427.

(19) Zhou, X.; Wang, B.; Sun, H.; Wang, C.; Sun, P.; Li, X.; Hu, X.; Lu, G. Template-free synthesis of hierarchical $ZnFe_2O_4$ yolk-shell microspheres for high-sensitivity acetone sensors. *Nanoscale* **2016**, *8*, 5446−5453.

(20) Zhou, X.; Li, X.; Sun, H.; Sun, P.; Liang, X.; Liu, F.; Hu, X.; Lu, G. Nanosheet-assembled $ZnFe_2O_4$ hollow microspheres for high-sensitive acetone sensor. *ACS Appl. Mater. Interfaces* **2015**, *7*, 15414−15421.

(21) Zhou, X.; Liu, J.; Wang, C.; Sun, P.; Hu, X.; Li, X.; Shimanoe, K.; Yamazoe, N.; Lu, G. Highly sensitive acetone gas sensor based on porous $ZnFe_2O_4$ nanospheres. *Sens. Actuators, B* **2015**, *206*, 577−583.

(22) Wang, Y.; Liu, F.; Yang, Q.; Gao, Y.; Sun, P.; Zhang, T.; Lu, G. Mesoporous $ZnFe_2O_4$ prepared through hard template and its acetone sensing properties. *Mater. Lett.* **2016**, *183*, 378−381.

(23) Zhang, G.; Li, C.; Cheng, F.; Chen, J. $ZnFe_2O_4$ tubes: Synthesis and application to gas sensors with high sensitivity and low-energy consumption. *Sens. Actuators, B* **2007**, *120*, 403−410.

(24) Oh, M. H.; Yu, T.; Yu, S.-H.; Lim, B.; Ko, K.-T.; Willinger, M.-G.; Seo, D.-H.; Kim, B. H.; Cho, M. G.; Park, J.-H.; Kang, K.; Sung, Y.-E.; Pinna, N.; Hyeon, T. Galvanic replacement reactions in metal oxide nanocrystals. *Science* **2013**, *340*, 964−968.

(25) Wang, X.; Feng, J.; Bai, Y.; Zhang, Q.; Yin, Y. Synthesis, properties, and applications of hollow micro-/nanostructures. *Chem. Rev.* **2016**, *116*, 10983−11060.

(26) Yu, L.; Wu, H. B.; Lou, X. W. Self-templated formation of hollow structures for electrochemical energy applications. *Acc. Chem. Res.* **2017**, *50*, 293−301.

(27) Zhou, L.; Zhuang, Z.; Zhao, H.; Lin, M.; Zhao, D.; Mai, L. Intricate hollow structures: controlled synthesis and applications in energy storage and conversion. *Adv. Mater.* **2017**, *29*, 1602914.

(28) Lai, X.; Li, J.; Korgel, B. A.; Dong, Z.; Li, Z.; Su, F.; Du, J.; Wang, D. General synthesis and gas-sensing properties of multiple-shell metal oxide hollow microspheres. *Angew. Chem., Int. Ed.* **2011**, *50*, 2738−2741.

(29) Lou, X. W.; Archer, L. A.; Yang, Z. Hollow micro-/nanostructures: synthesis and applications. *Adv. Mater.* **2008**, *20*, 3987−4019.

(30) Qi, J.; Lai, X.; Wang, J.; Tang, H.; Ren, H.; Yang, Y.; Jin, Q.; Zhang, L.; Yu, R.; Ma, G.; Su, Z.; Zhao, H.; Wang, D. Multi-shelled hollow micro- nanostructures. *Chem. Soc. Rev.* **2015**, *44*, 6749−6773.

(31) Zhao, S.-N.; Song, X.-Z.; Song, S.-Y.; Zhang, H.-j. Highly efficient heterogeneous catalytic materials derived from metal-organic framework supports/precursors. *Coord. Chem. Rev.* **2017**, *337*, 80−96.

(32) Cao, X.; Tan, C.; Sindoro, M.; Zhang, H. Hybrid micro- nanostructures derived from metal−organic frameworks preparation and applications in energy storage and conversion. *Chem. Soc. Rev.* **2017**, *46*, 2660−2677.

(33) Han, L.; Yu, X.-Y.; Lou, X. W. Formation of prussian-blue-analog nanocages via a direct etching method and their conversion into Ni-Co-mixed oxide for enhanced oxygen evolution. *Adv. Mater.* **2016**, *28*, 4601−4605.

(34) Sun, D.; Ye, L.; Sun, F.; Garcia, H.; Li, Z. From mixed-metal MOFs to carbon-coated core-shell metal alloy@metal oxide solid solutions: transformation of Co/Ni-MOF-74 to Co_xNi_{1-x}@$Co_yNi_{1-y}O$@C for the oxygen evolution reaction. *Inorg. Chem.* **2017**, *56*, 5203−5209.

(35) Zou, K. Y.; Liu, Y. C.; Jiang, Y. F.; Yu, C. Y.; Yue, M. L.; Li, Z. X. Benzoate acid-dependent lattice dimension of Co-MOFs and MOF-derived CoS_2@CNTs with tunable pore diameters for supercapacitors. *Inorg. Chem.* **2017**, *56*, 6184−6196.

(36) Qu, F.; Jiang, H.; Yang, M. MOF-derived Co_3O_4/$NiCo_2O_4$ double-shelled nanocages with excellent gas sensing properties. *Mater. Lett.* **2017**, *190*, 75−78.

(37) Qu, F.; Jiang, H.; Yang, M. Designed formation through a metal organic framework route of ZnO/$ZnCo_2O_4$ hollow core−shell nanocages with enhanced gas sensing properties. *Nanoscale* **2016**, *8*, 16349−16356.

(38) Koo, W. T.; Choi, S. J.; Jang, J. S.; Kim, I. D. Metal-organic framework templated synthesis of ultrasmall catalyst loaded ZnO/$ZnCo_2O_4$ hollow spheres for enhanced gas sensing properties. *Sci. Rep.* **2017**, *7*, 45074.

(39) Song, X.-Z.; Qiao, L.; Sun, K.-M.; Tan, Z.; Ma, W.; Kang, X.-L.; Sun, F.-F.; Huang, T.; Wang, X.-F. Triple-shelled ZnO/$ZnFe_2O_4$ heterojunctional hollow microspheres derived from Prussian Blue analogue as high-performance acetone sensors. *Sens. Actuators, B* **2017**, DOI: 10.1016/j.snb.2017.10.081.

DOI: 10.1021/acs.inorgchem.7b02425
Inorg. Chem. XXXX, XXX, XXX−XXX

(40) Zhang, W.; Jiang, X.; Zhao, Y.; Carné-Sánchez, A.; Malgras, V.; Kim, J.; Kim, J. H.; Wang, S.; Liu, J.; Jiang, J.-S.; Yamauchi, Y.; Hu, M. Hollow carbon nanobubbles: monocrystalline MOF nanobubbles and their pyrolysis. *Chem. Sci.* **2017**, *8*, 3538−3546.
(41) Liu, W.; Huang, J.; Yang, Q.; Wang, S.; Sun, X.; Zhang, W.; Liu, J.; Huo, F. Multi-shelled hollow metal−organic frameworks. *Angew. Chem., Int. Ed.* **2017**, *56*, 5512−5516.
(42) Zhang, Z.; Chen, Y.; Xu, X.; Zhang, J.; Xiang, G.; He, W.; Wang, X. Well-defined metal-organic framework hollow nanocages. *Angew. Chem., Int. Ed.* **2014**, *53*, 429−433.
(43) Oh, M.; Mirkin, C. A. Chemically tailorable colloidal particles from infinite coordination polymers. *Nature* **2005**, *438*, 651−654.
(44) Yu, H.; Fan, H.; Wu, X.; Wang, H.; Luo, Z.; Tan, H.; Yadian, B.; Huang, Y.; Yan, Q. Diffusion induced concave Co_3O_4@$CoFe_2O_4$ hollow heterostructures for high performance lithium ion battery anode. *Energy Storage Materials* **2016**, *4*, 145−153.
(45) Epling, W. S.; Hoflund, G. B.; Weaver, J. F.; Tsubota, S.; Haruta, M. Surface characterization study of Au α-Fe_2O_3 and Au Co_3O_4 low-temperature CO oxidation catalysts. *J. Phys. Chem.* **1996**, *100*, 9929−9934.
(46) Hu, D.; Han, B.; Deng, S.; Feng, Z.; Wang, Y.; Popovic, J.; Nuskol, M.; Wang, Y.; Djerdj, I. Novel mixed phase SnO_2 nanorods assembled with SnO_2 nanocrystals for enhancing gas-sensing performance toward isopropanol gas. *J. Phys. Chem. C* **2014**, *118*, 9832−9840.
(47) Zhang, J.; Song, J.-M.; Niu, H.-L.; Mao, C.-J.; Zhang, S.-Y.; Shen, Y.-H. $ZnFe_2O_4$ nanoparticles: Synthesis, characterization, and enhanced gas sensing property for acetone. *Sens. Actuators, B* **2015**, *221*, 55−62.
(48) Wang, S.; Gao, X.; Yang, J.; Zhu, Z.; Zhang, H.; Wang, Y. Synthesis and gas sensor application of $ZnFe_2O_4$−ZnO composite hollow microspheres. *RSC Adv.* **2014**, *4*, 57967−57974.
(49) Li, X.; Wang, C.; Guo, H.; Sun, P.; Liu, F.; Liang, X.; Lu, G. Double-shell architectures of $ZnFe_2O_4$ nanosheets on ZnO hollow spheres for high-performance gas sensors. *ACS Appl. Mater. Interfaces* **2015**, *7*, 17811−17818.
(50) Yamazoe, N.; Sakai, G.; Shimanoe, K. Oxide Semiconductor gas sensors. *Catal. Surv. Asia* **2003**, *7*, 63−75.
(51) Bai, J.; Zhou, B. Titanium dioxide nanomaterials for sensor applications. *Chem. Rev.* **2014**, *114*, 10131−10176.

DOI: 10.1021/acs.inorgchem.7b02425
Inorg. Chem. XXXX, XXX, XXX−XXX